
GAN-BASED VERTICAL FEDERATED LEARNING FOR LABEL PROTECTION IN BINARY CLASSIFICATION

Yujin Han
 Department of Biostatistics
 Yale University
 New Haven, CT 06520, USA
 yujin.han@yale.edu

Leying Guan
 Department of Biostatistics
 Yale University
 New Haven, CT 06520, USA
 leying.guan@yale.edu

May 18, 2023

ABSTRACT

Split learning (splitNN) has emerged as a popular strategy for addressing the high computational costs and low modeling efficiency in Vertical Federated Learning (VFL). However, despite its popularity, vanilla splitNN lacks encryption protection, leaving it vulnerable to privacy leakage issues, especially Label Leakage from Gradients (LLG). Motivated by the LLG issue resulting from the use of labels during training, we propose the Generative Adversarial Federated Model (GAFM), a novel method designed specifically to enhance label privacy protection by integrating splitNN with Generative Adversarial Networks (GANs). GAFM leverages GANs to indirectly utilize label information by learning the label distribution rather than relying on explicit labels, thereby mitigating LLG. GAFM also employs an additional cross-entropy loss based on the noisy labels to further improve the prediction accuracy. Our ablation experiment demonstrates that the combination of GAN and the cross-entropy loss component is necessary to enable GAFM to mitigate LLG without significantly compromising the model utility. Empirical results on various datasets show that GAFM achieves a better and more robust trade-off between model utility and privacy compared to all baselines across multiple random runs. In addition, we provide experimental justification to substantiate GAFM’s superiority over splitNN, demonstrating that it offers enhanced label protection through gradient perturbation relative to splitNN.

1 Introduction

Federated learning trains algorithms across multiple decentralized remote devices or siloed data centers without sharing sensitive data. There are three types of federated learning depending on the data partitioning methods used: horizontal federated learning (HFL), vertical federated learning (VFL), and federated transfer learning [36]. VFL partitions the data vertically, where local participants have datasets with the same sample IDs but different features [17]. With stricter data privacy regulations like CCPA1 [24] and GDPR3 [31], VFL is a viable solution for enterprise-level data collaborations, as it facilitates collaborative training and privacy protection. However, VFL faces challenges in terms of high memory costs and processing time overheads, attributed to the complex cryptographic operations employed to provide strong privacy guarantees [38], including additive homomorphic encryption [17] and secure multi-party computation [22], which are computationally intensive. To address these issues, split learning [14, 30, 2] has emerged as an efficient solution, allowing multiple participants to jointly train federated models without encrypting intermediate results, thus reducing computational costs. SplitNN [6], which applies the concept of split learning to neural networks, has been used successfully in the analysis of medical data [26, 15].

Split learning, while reducing computational costs, poses substantial privacy risks due to the absence of encryption protection for model privacy. One specific privacy risk is Label Leakage from Gradients (LLG) [33], in which gradients flowing from the label party to the non-label (only data) party can expose the label information [10, 40, 32]. LLG is susceptible to exploitation for stealing label information in binary classification and has limited proposed solutions to address it. Recent work by Li et al. [21] indicates that *in binary classification, the gradient norm of positive instances*

is generally larger than negative ones, which could potentially enable attackers to easily infer sample labels from intermediate gradients in splitNN. Despite the fact that binary classification is widely used in various federated scenarios, such as healthcare, finance, credit risk, and smart cities [9, 5, 8, 39], and is vulnerable to LLG, limited research has been conducted on addressing the LLG issue in binary classification. Previous studies [6, 10, 29, 25] have focused mainly on securing the data information of non-label parties, while ignoring the risk of leaking highly sensitive label information of the label party. Therefore, it is critical to address how splitNN can resist LLG in binary classification tasks.

In this work, in order to prevent inferring sample labels from the gradient calculation, we introduce a novel Generative Adversarial Federated Model (GAFM), which synergistically combines the vanilla splitNN architecture with Generative Adversarial Networks (GANs) to indirectly incorporate labels into the model training process. Specifically, the GAN discriminator within GAFM allows federated participants to learn a prediction distribution that closely aligns with the label distribution, effectively circumventing the direct use of labels inherent in the vanilla SplitNN approach. Moreover, to counteract the potential degradation of model utility induced by GANs, we enhance our method by incorporating additional label information via an additional cross-entropy loss, which encourages the intermediate results generated by the non-label party and the labels with added noise provided by the label party to perform similarly. The entire framework of the proposed GAFM and the training procedures is displayed in Figure 1. Our contributions are highlighted as follows.

- We propose a novel GAN-based approach, called GAFM, which combines vanilla splitNN with GAN to mitigate LLG in binary classification (section 3.2). Our analysis in section 3.4 demonstrates that GAFM protects label privacy by generating more mixed intermediate gradients through the mutual gradient perturbation of both the GAN and cross-entropy components.
- We enrich the existing gradient-based label stealing attacks by identifying two additional simple yet practical attack methods, namely mean attack and median attack in section 3.5. The experimental results in section 4.2.1 demonstrate that our new attacks are more effective in inferring labels than the existing ones.
- We evaluate the effectiveness of GAFM on various datasets. Empirical results in section 4 show that GAFM mitigates LLG without significant model utility degradation and the performance of GAFM across different random seeds is more stable compared to baselines. We also provide additional insights based on the ablation experiment (section 4.2.2) to demonstrate the necessity of combining both the GAN and cross-entropy components in GAFM. Compared to the stable balance between utility and privacy that can be achieved by using both components, GAFM with only the GAN component provides enhanced privacy protection at the cost of reduced utility, while GAFM with only the cross-entropy component delivers superior utility but offers limited privacy protection.

2 Related Work

SplitNN-driven Vertical Partitioning. SplitNN enables multiple participants to train a distributed model without sharing their data and encrypting intermediate results [14, 30, 6]. In SplitNN, each passive participant trains a partial neural network locally, and the layer at which the label and non-label participants share information is called the cut layer. At the cut layer of SplitNN, each non-label party trains a fixed portion of the neural network locally and shares intermediate results with the label party. The label party then aggregates these intermediate results and implements backward propagation to update the local parameters of each non-label party. There are several methods of aggregation, such as element-wise average, element-wise maximum, element-wise sum, element-wise multiplication, concatenation, and non-linear transformation [6].

Label privacy protection via random gradient perturbation. To address the issue of LLG through intermediate gradients at the cut layer, one possible solution is to introduce randomness to the intermediate gradients, which has been utilized in HFL [1, 12, 19]. **Marvell** [21] is a random perturbation approach specifically designed for binary classification tasks. Marvell protects label privacy by perturbing the intermediate gradients and aims to find the optimal zero-centered Gaussian perturbations that minimize the sum of KL divergences between two perturbed distributions, while adhering to a budget constraint on the amount of perturbation added:

$$\begin{aligned} & \min_{W^{(0)}, W^{(1)}} \text{KL}(\tilde{\mathbb{P}}^1 \parallel \tilde{\mathbb{P}}^0) + \text{KL}(\tilde{\mathbb{P}}^0 \parallel \tilde{\mathbb{P}}^1) \\ & \text{s.t. } \text{ptr}(\Sigma_0) + (1 - p)\text{tr}(\Sigma_1) \leq P, \end{aligned} \tag{1}$$

where $\tilde{\mathbb{P}}^k$ is the distribution of perturbed intermediate gradients from k after convolution with the Gaussian noise $W^{(k)} = \mathcal{N}(0, \Sigma_k)$, $k = 0, 1$, p is the weight and P is the budget for how much random perturbation Marvell is allowed to add. As the intermediate gradients with different labels become less distinguishable, it becomes more difficult for attackers to infer labels from gradients.

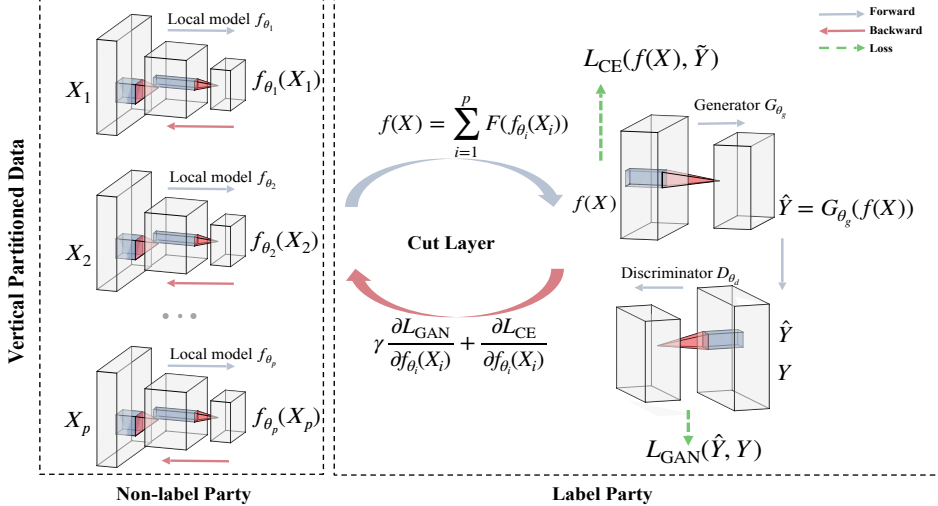


Figure 1: An illustration of **Generative Adversarial Federated Model (GAFM)** with P non-label parties and one label party. Each non-label participant uses its local model f_{θ_p} to extract feature information $f_{\theta_p}(X_p)$ from its local data X_p , where θ_p is denoted as the local model parameter of the p th non-label participant. The label party aggregates all feature information in the cut layer to obtain intermediate results $f(X)$, which are then used as input to the generator G_{θ_g} with θ_g being the generator model parameter. The label party then trains the generator G_{θ_g} and discriminator D_{θ_d} adversarially using the true label Y and the prediction \hat{Y} (the output of G_{θ_g}), where θ_d is the discriminator model parameter. To incorporate additional true label information for improving the prediction accuracy, an additional cross-entropy loss L_{CE} is introduced. Section 3 provides more details on GAFM.

Max Norm [21] is an improved heuristic approach of adding zero-mean Gaussian noise with non-isotropic and example-dependent covariance. More concretely, for the intermediate gradient \mathbf{g}_j of data point j , Max Norm adds the zero-mean Gaussian noise η_j to it with the covariance as:

$$\sigma_j = \sqrt{\frac{\|\mathbf{g}_{\max}\|_2^2}{\|\mathbf{g}_j\|_2^2} - 1}, \quad (2)$$

where $\|\mathbf{g}_{\max}\|_2^2$ is the largest squared 2-norm in a batch. Max Norm is a simple, straightforward, and parameter-free perturbation method. But it does not have strong theoretical motivation and cannot guarantee to defend unknown attacks [21].

GAN in Federated Learning. Previously, researchers have combined GAN and HFL for various purposes, including three directions in HFL: (1) generating malicious attacks [18, 34], (2) training high-quality GAN across distributed data under privacy constraints [16, 27, 23], and (3) protecting client data privacy [35], known as FedCG. In FedCG, each client train a classifier predicting the response Y using Z extracted from the original feature X , and a conditional GAN that learns the conditional distribution of Z given Y . The classifiers and generators (instead of the extracted Z) from different clients are then passed to the server for updating the common model. FedCG has been shown to effectively protect clients' data privacy in HFL. These previous works have demonstrated the promising role of GAN in HFL, but to the best of our knowledge, there has been no prior work investigating the GAN model for label protection in VFL.

3 Generative Adversarial Federated Model (GAFM)

In this section, we first introduce the split learning problem for binary classification, including its associated notations. We then provide a detailed description of the GAFM method, along with a discussion on GAFM's parameter selection. Additionally, we explain how GAFM offers better label privacy protection than vanilla splitNN and propose new label stealing methods to evaluate GAFM's privacy protection ability in subsequent experiments.

3.1 Problem setting and notation

We consider the joint training of one label party and P non-label parties for binary classification tasks over the domain $\mathcal{X} \times \{0, 1\}$. Each non-label party p possesses one local model $f_{\theta_p} : \mathcal{X} \rightarrow \mathbb{R}^d$ where θ_p is the local model parameter of non-label party p and the local data $X_p \in \mathcal{X}$. In vanilla splitNN, the label party owns the transformation function $F : \mathbb{R}^d \rightarrow \mathbb{R}^d$ for feature aggregation in the cut layer, the logit function $h : \mathbb{R}^d \rightarrow \mathbb{R}$ for prediction, and each example's label $y \in \{0, 1\}$. In contrast, in GAFM, the transformation function F for feature aggregation remains with the label party, while the logit function h is replaced by the generator $G_{\theta_g} : \mathbb{R}^d \rightarrow \mathbb{R}$ where θ_g is the generator model parameter. Furthermore, GAFM includes an additional discriminator $D_{\theta_d} : \mathbb{R} \rightarrow \mathbb{R}$ where θ_d is the discriminator model parameter.

3.2 GAFM framework

In this section, we provide a detailed description of the GAFM framework. As illustrated in Figure 1, each non-label party p in GAFM utilizes its local model f_{θ_p} to extract local feature information from its local data X_p and sends it to the label party. In the cut layer, the label party aggregates the feature information from all non-label parties to obtain the intermediate result $f(X) = F(\sum_p f_{\theta_p}(X_p))$, where $F(\cdot)$ is a known transformation function, such as the identity function. The label party takes the intermediate result $f(X)$ as input to the generator G_{θ_g} , and the output of G_{θ_g} is treated as the prediction \hat{Y} . Then, the label party adversarially trains both the generator G_{θ_g} and the discriminator D_{θ_d} with guidance from the true label Y and the prediction \hat{Y} . The GAN loss L_{GAN} between G_{θ_g} and D_{θ_d} is defined in equation 3, which quantifies the distance between the prediction \hat{Y} and the ground truth Y distribution by employing the Wasserstein-1 distance [20]:

$$L_{\text{GAN}}(\theta_d, \theta_g; \varepsilon) = \mathbb{E}_Y [D_{\theta_d}(Y + \varepsilon)] - \mathbb{E}_X [D_{\theta_d}(\hat{Y})], \quad (3)$$

where $\varepsilon \sim N(0, \sigma^2)$ is a small additive Gaussian noise so that $Y + \varepsilon$ has a continuous support. The Wasserstein loss, which encourages the predicted distribution to closely align with the empirical response, is applicable to classification tasks [11].

To improve the prediction accuracy in GAFM, we introduce an additional cross-entropy (CE) loss, which measures the distance between the intermediate result $f(X)$ and the randomized response \tilde{Y} . The randomized response \tilde{Y} is defined as:

$$\tilde{Y} = \begin{cases} 0.5 + u; & Y = 1 \\ 0.5 - u; & Y = 0, \end{cases} \quad (4)$$

where the random variable $u \sim \text{Uniform}(0, \Delta)$ and the hyperparameter $\Delta \in [0, 0.5]$. The randomized response \tilde{Y} replaces the original response Y , which enhances label protection against LLG. Setting $\Delta = 0$ removes any label information from the original data, while $\Delta > 0$ allows \tilde{Y} to guide the classifier without excessive label leakage from CE loss. The use of a randomized response is a departure from previous work, which used the true label Y and encountered issues with label leakage. Following the equation 4, the CE loss is:

$$L_{\text{CE}}(\Theta; u) = -\mathbb{E}_{XY} [\tilde{Y} \log(\sigma(f(X))) + (1 - \tilde{Y}) \log(1 - \sigma(f(X)))] \quad (5)$$

where $\Theta = \{\theta_1, \dots, \theta_P\}$ is the local model parameter set and the function σ is the sigmoid function. In particular, $\tilde{Y} \in \mathbb{R}$ and $f(X) \in \mathbb{R}^d$, where d is an arbitrary dimension. When $d \neq 1$, $f(X)$ needs to be summed along the d -dimension to be consistent with the dimension of \tilde{Y} .

Combine the L_{GAN} defined in equation 3 and the L_{CE} defined in equation 5, we obtain the full loss of GAFM, as given by equation (6):

$$\min_{\theta_g, \theta_p} \max_{\theta_d} L_{\text{GAFM}}(\theta_d, \theta_g, \Theta; \varepsilon, u, \gamma) = \gamma L_{\text{GAN}}(\theta_d, \theta_g; \varepsilon) + L_{\text{CE}}(\Theta; u), \quad (6)$$

where the loss weight hyperparameter $\gamma > 0$.

Following the parameter update sequence of Wasserstein-based GANs [3], GAFM enables the label party to update the discriminator parameter θ_d first, followed by updating the generator parameter θ_g . Then, the non-label parties update local model parameters Θ :

- (1) Update θ_d to maximize the GAN loss: $\theta_d \leftarrow \arg \max_{\theta_d} L_{\text{GAN}}(\theta_d, \theta_g; \varepsilon)$, given θ_g, Θ .
- (2) Update θ_g to minimize the GAN loss: $\theta_g \leftarrow \arg \min_{\theta_g} L_{\text{GAN}}(\theta_d, \theta_g; \varepsilon)$, given θ_d, Θ .

(3) Update Θ to minimize GAFM loss: $\Theta \leftarrow \arg \min_{\Theta} L_{\text{GAFM}}(\theta_d, \theta_g, \Theta; \varepsilon, u)$, given θ_d, θ_g .

We employ the Adam optimizer with learning rates α_d , α_g , and α_p , respectively, to implement the aforementioned procedures. To satisfy the Lipschitz constraint of the discriminator in Wasserstein-based GANs [4, 13], we apply weight clipping to discriminator parameters θ_d . This operation restricts the parameters θ_d to the interval $[-c, c]$, where c is a hyperparameter. Further details regarding the algorithm can be found in Algorithm A.1.

3.3 Selection of GAFM hyperparameters

GAFM incorporates three crucial parameters: σ , γ , and Δ . The parameter σ introduces Gaussian noise $\varepsilon \sim N(0, \sigma^2)$ into the ground truth Y distribution to render it continuously supported. The default value of σ can be set to 0.01, and the Appendix D.1 shows that GAFM is insensitive to different values of σ . Specifically, a broad range of $\sigma \in [0.01, 1]$ yields comparable empirical results.

The tuning of the loss weight hyperparameter γ in GAFM can be challenging due to the vanishing gradient issue of the unnormalized GAN loss gradients [4, 13]. To address this issue, we introduce normalization techniques for the gradients of the GAN loss and the CE loss, respectively. This normalization technique in GAFM alleviates the vanishing gradient problem, making it feasible to determine the hyperparameter γ . Appendix D.2 provides insights on selecting the appropriate value of γ for different datasets. Our experiments demonstrate that an effective approach to determine γ is to adjust it to balance the magnitude between the average value of the GAN loss gradient and the average value of the CE loss gradient. Additional details on the selection of Δ are discussed in Appendix D.2.

We also propose a simple yet effective approach for determining the randomized response-related hyperparameter Δ . Specifically, we train GAFM with different values of Δ on a 10% subset of the data and select the optimal parameter based on its utility and privacy. The analysis in Appendix D.3 shows that the Δ selected based on the subset is very close to or even equal to the optimal parameter selected on the full dataset. Additional details on the selection of Δ are discussed in Appendix D.3.

3.4 Why does GAFM protect against LLG?

In this section, we show that GAFM provides stronger privacy protection against LLG by generating more mixed intermediate gradients compared to vanilla splitNN. Specifically, the proposition 3.1 from the work [21] states that the KL divergence between the intermediate gradients of two classes sets an upper bound on the amount of label information an attacker can obtain via any LLG attacks.

Proposition 3.1. [21] *Let $\tilde{\mathbb{P}}^1$ and $\tilde{\mathbb{P}}^0$ be perturbed distributions for intermediate gradients of classes 1 and 0, and be continuous with respect to each other. For $\epsilon \in [0, 4]$,*

$$\begin{aligned} \text{KL}(\tilde{\mathbb{P}}^1 \parallel \tilde{\mathbb{P}}^0) + \text{KL}(\tilde{\mathbb{P}}^0 \parallel \tilde{\mathbb{P}}^1) &\leq \epsilon \\ \text{implies } \max_r \text{AUC}_r &\leq \frac{1}{2} + \frac{\sqrt{\epsilon}}{2} - \frac{\epsilon}{8}, \end{aligned} \tag{7}$$

where r is any LLG attack, and AUC_r represents the achieved AUC using r .

The proposition 3.1 proposes that models with more mixed intermediate gradients (meaning a smaller sum of KL divergences from the two classes) may imply a smaller upper bound ϵ , which results in a smaller amount of available label information and better protection against LLG. Therefore, we indirectly demonstrate GAFM's superior label privacy protection ability by showing that GAFM has more mixed intermediate gradients than vanilla splitNN. Figure 2 illustrates the intermediate gradients of vanilla splitNN, GAFM, the GAN loss gradient of GAFM, and the CE loss gradient of GAFM on the IMDB dataset from left to right. We observe that GAFM has more mixed intermediate gradients compared to vanilla splitNN. Furthermore, the gradient class centers of the GAN loss gradient and the CE loss gradient differ in opposite directions, leading to mutual cancellation in the final gradient for GAFM. We further provide a heuristic justification in Appendix B to explain the observed discrepancy in the directions of the GAN loss gradient class centers and the CE loss gradient class centers shown in Figure 2.

3.5 Label stealing attacks

In this section, we introduce three gradient-based label stealing attacks which are applied in subsequent experiments to evaluate the effectiveness of GAFM in mitigating LLG.

Norm Attack. The norm attack [21] is a simple heuristic for black-box attacks that can be used for label inference in binary classification tasks. The attack is based on the observation that the gradient norm $\|\mathbf{g}\|_2$ of positive instances

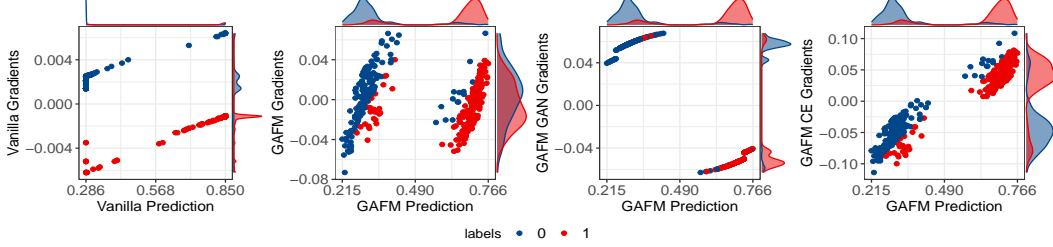


Figure 2: **Comparison of Prediction vs. Intermediate Gradients** between vanilla splitNN and GAFM on IMDB. The figure 2 displays, from left to right, the intermediate gradients of vanilla splitNN, GAFM, the GAN loss gradient of GAFM, and the CE loss gradient of GAFM. Our observations show that (1) GAFM has more mixed intermediate gradients compared to vanilla splitNN; (2) the gradient class centers from the GAN loss gradient and the CE loss gradient differ in opposite directions, leading to mutual perturbation in the final gradient for GAFM. Observations from Spambase, Criteo, and ISIC in Appendix C.1 are consistent with those from the IMDB dataset.

tends to differ from that of negative instances, especially with unbalanced datasets. Thus, the gradient norm $\|\mathbf{g}\|_2$ can be a strong predictor of labels.

Previous research indicates that vanilla SplitNN gradients tend to form two clusters based on the cosine similarity sign, leading to the development of cosine attacks [21]. In the case of GAFM, although the relationship between the sign and the cluster of gradients may not be as straightforward, attackers can still attempt to make attacks based on proximity to a cluster. To achieve this goal, we propose mean-based attacks and further enhance robustness against outliers in gradients by introducing median-based attacks.

Mean Attack. We propose a mean-based attack as a heuristic for black-box attacks that exploits clustering structures in gradients. Assuming that attackers know the gradient centers of class 0 and class 1, denoted as μ_0 and μ_1 , mean-based attacks assign a sample i to the cluster that its intermediate gradient \mathbf{g}_i is closer to:

$$y_i = \begin{cases} 1, & \text{if } \|\mathbf{g}_i - \mu_1\|_2 \leq \|\mathbf{g}_i - \mu_0\|_2 \\ 0, & \text{otherwise.} \end{cases} \quad (8)$$

Median Attack. We propose a median-based attack, which is similar to the mean-based attack but more robust to outliers. Assuming that attackers know the gradient medians of class 0 and class 1, denoted as \mathbf{m}_0 and \mathbf{m}_1 , median-based attacks assign a sample i to the cluster that its intermediate gradient \mathbf{g}_i is closer to:

$$y_i = \begin{cases} 1, & \text{if } \|\mathbf{g}_i - \mathbf{m}_1\|_2 \leq \|\mathbf{g}_i - \mathbf{m}_0\|_2 \\ 0, & \text{otherwise.} \end{cases} \quad (9)$$

4 Experiments

In this section, we first provide a comprehensive description of the experimental setup, including the datasets, model architectures, baselines, and evaluation metrics. Then, we present the experimental results that showcase the utility and privacy performance of GAFM. Furthermore, we conduct an ablation study to elucidate the contribution of each component of GAFM.

4.1 Experiment Setup

Datasets. Our approach is evaluated on four real-world binary classification datasets: Spambase¹, which is used for spam email discrimination; IMDB², a binary sentiment classification dataset consisting of 50,000 highly polar movie reviews; Criteo³, an online advertising prediction dataset with millions of examples; and ISIC⁴, a healthcare image dataset for skin cancer prediction. Criteo and ISIC are two datasets with severely imbalanced label distributions,

¹<https://archive.ics.uci.edu/ml/datasets/spambase>

²<https://www.kaggle.com/datasets/uciml/default-of-credit-card-clients-dataset>

³<https://www.kaggle.com/c/criteo-display-ad-challenge>

⁴<https://www.kaggle.com/datasets/nodoubtome/skin-cancer9-classesisic>

Table 1: **Dataset statistics and model architectures.** Different local model architectures f_{Θ} are considered for different datasets. 2-layer DNNs are sufficient as the generator G_{θ_g} and discriminator D_{θ_d} since their inputs are simple linear embeddings.

| Dataset | Positive Instance Proportion | f_{Θ} | G_{θ_g} | D_{θ_d} |
|----------|------------------------------|---------------|----------------|----------------|
| Spambase | 39.90% | 2-layer DNN | | |
| IMDB | 50.00% | 3-layer DNN | 2-layer | 2-layer |
| Criteo | 22.66% | WDL Model [7] | DNN | DNN |
| ISIC | 1.76% | 6-layer CNN | | |

which have been used in the works of Max Norm and Marvell [21]. Furthermore, we consider another two class-balanced datasets, Spambase and IMDB, to evaluate the performance of GAFM under different class setting. Additional information regarding the datasets and data preprocessing can be found in Table 1 and Appendix E.1.

Model Architecture. We consider the two-party split learning setting used by Marvell, where the label party has access only to the label and the non-label party has access only to the data. In Section C.2, we also present the utility and privacy protection results of all methods under a multi-client scenario with three non-label parties. Table 1 lists the model architectures of local models f_{Θ} , generator G_{θ_g} , and discriminator D_{θ_d} used for each dataset. Similar to Marvell, we employ a Wide and Deep model [7] for Criteo and a 6-layer CNN for ISIC as the local models f_{Θ} . More details on model architectures and training can be found in Appendices E.2 and E.3.

Baselines. We compare the utility and privacy of GAFM with Marvell [21], Max Norm [21] and vanilla splitNN.

Evaluation Metrics. We employ the Area Under Curve (AUC) metric to evaluate model utility and the leak AUC to assess model privacy protection. Differential privacy is not considered as a leakage measure, as it is not applicable to example-specific and example-aware settings like VFL [21]. The leak AUC [21, 37, 28] is defined as the AUC achieved by using specific attacks. A high leak AUC value, closer to 1, indicates that the attacker can accurately recover labels, while a low leak AUC value, around 0.5, suggests that the attacker has less information for inferring labels. To prevent simple label flipping from resulting in a higher leak AUC, we modify the leak AUC as shown in equation 10 for a predefined attack by flipping the label assignment if doing so results in a higher AUC:

$$\text{leakAUC} \leftarrow \max(\text{leakAUC}, 1 - \text{leakAUC}) \quad (10)$$

4.2 Results

This section presents AUC and leak AUC to demonstrate the trade-off between privacy and utility of GAFM. We also report the results of the ablation study, which illustrates the contribution of each component of GAFM. Each method is executed 10 times with unique random seeds and train-test splits. Further experiment details can be found in the Appendix E.

4.2.1 Evaluation of utility and privacy

Table 2 illustrates the average AUC and average leak AUC across four datasets. GAFM achieves comparable classification AUC with Vanilla and Max Norm, but demonstrates lower leak AUC, indicating its effectiveness in protecting label privacy and defending against LLG. Compared to Marvell, GAFM achieves slightly higher average AUC on most datasets while maintaining comparable leak AUC. Importantly, GAFM demonstrates more stable performance than Marvell, with reduced variance between the worst and best AUC across different random seeds. This could be attributed to Marvell’s gradient perturbation technique, which introduces Gaussian noise to intermediate gradients and can lead to unstable performance, as evidenced by the highly fluctuating leak AUC of Criteo and ISIC shown in the Marvell paper [21]. Additionally, we observe that our proposed mean attack and median attack achieve higher leak AUC on all four datasets compared to the norm attack. This indicates that mean attack and median attack are more effective gradient-based attacks for label stealing compared to the existing norm attack.

In conclusion, Table 2 demonstrates GAFM’s improvement in privacy protection over Vanilla and Max Norm, as well as its improvement in utility and stability compared to Marvell. GAFM achieves better trade-off between utility and privacy compared to the baseline models.

4.2.2 Ablation study

Figure 3 compares GAFM with two ablated versions: GAFM with only GAN loss (GAN-only) and GAFM with only CE loss (CE-only). The results show that GAFM strikes a better balance between utility and privacy across various

Table 2: **Comparison of utility and privacy between GAFM and baselines.** Compared to Vanilla and Max Norm, GAFM achieves lower leak AUC at similar AUC, demonstrating its effectiveness in protecting label privacy. Compared to Marvell, GAFM demonstrates comparable and even better utility and privacy protection on most datasets, while also exhibiting greater stability with reduced variance between the best and worst AUC across different random seeds. Table 2 illustrates that GAFM offers a better and more stable trade-off between utility and privacy compared to all baselines.

| Dataset | Method | Utility | | | Privacy | | |
|----------|----------|----------|-----------|----------|-------------|-------------|---------------|
| | | Avg. AUC | Worst AUC | Best AUC | Norm Attack | Mean Attack | Median Attack |
| Spambase | GAFM | 0.93 | 0.91 | 0.95 | 0.56±0.04 | 0.67±0.05 | 0.66±0.05 |
| | Marvell | 0.71 | 0.59 | 0.82 | 0.53±0.02 | 0.70±0.01 | 0.70±0.01 |
| | Max Norm | 0.95 | 0.95 | 0.95 | 0.83±0.11 | 1.00±0.00 | 0.91±0.00 |
| | Vanilla | 0.95 | 0.95 | 0.96 | 0.85±0.07 | 1.00±0.00 | 0.91±0.00 |
| IMDB | GAFM | 0.88 | 0.88 | 0.89 | 0.52±0.01 | 0.60±0.01 | 0.60±0.01 |
| | Marvell | 0.80 | 0.71 | 0.89 | 0.52±0.01 | 0.73±0.01 | 0.73±0.01 |
| | Max Norm | 0.89 | 0.89 | 0.90 | 0.82±0.09 | 1.00±0.00 | 0.99±0.01 |
| | Vanilla | 0.89 | 0.89 | 0.90 | 0.82±0.09 | 1.00±0.00 | 0.99±0.01 |
| Criteo | GAFM | 0.67 | 0.64 | 0.73 | 0.68±0.06 | 0.80±0.09 | 0.77±0.05 |
| | Marvell | 0.70 | 0.65 | 0.76 | 0.76±0.08 | 0.86±0.08 | 0.78±0.04 |
| | Max Norm | 0.69 | 0.65 | 0.72 | 0.92±0.01 | 0.83±0.09 | 0.82±0.00 |
| | Vanilla | 0.72 | 0.69 | 0.77 | 0.92±0.06 | 0.91±0.11 | 0.82±0.00 |
| ISIC | GAFM | 0.68 | 0.66 | 0.69 | 0.62±0.09 | 0.66±0.15 | 0.68±0.11 |
| | Marvell | 0.64 | 0.51 | 0.69 | 0.65±0.04 | 0.69±0.01 | 0.66±0.01 |
| | Max Norm | 0.76 | 0.72 | 0.82 | 0.99±0.01 | 1.00±0.00 | 0.77±0.00 |
| | Vanilla | 0.77 | 0.73 | 0.82 | 0.99±0.01 | 1.00±0.00 | 0.78±0.00 |

datasets. In contrast, the CE-only model exhibits large variations in privacy protection, while the GAN-only model consistently performs poorly in terms of model utility. Specifically, except for the Spambase dataset, the CE-only model shows extremely high leak AUCs on all other datasets, particularly on IMDB and ISIC datasets, where the mean and median attack leak AUCs reach 0.7 or even higher. While the GAN-only model achieves low leak AUC across all four datasets, its classification AUC is inferior to that of GAFM, which benefits from the guidance provided by the CE component. Particularly, on the IMDB and Criteo datasets, both GAFM and CE-only models maintain a classification AUC above 0.7, compared to around 0.5 achieved by the GAN-only model. These results highlight the necessity of combining GAN and CE components to endow GAFM with stable mitigation to LLG without compromising utility.

5 Discussion

We propose the Generative Adversarial Federated Model (GAFM), a novel method for binary classification tasks in VFL. Empirical experiments on four datasets demonstrate that GAFM is a promising method for effectively mitigating LLG. Unlike Marvell and Max Norm, which use noisy intermediate gradients to improve gradient mixing between the label and non-label parties, GAFM takes a different approach. By incorporating both the GAN loss and CE loss, we observed improved gradient mixing in GAFM compared to vanilla splitNN. Our analysis further reveals that GAFM’s ability to defend against LLG is attributed to the mutual gradient perturbation of the GAN loss and the CE loss.

Limitation and future work. Although heuristic proof and additional experiments are provided to explain GAFM’s privacy protection capabilities arise from the mutually perturbing gradients generated by the GAN and CE components, GAFM is not as rigorous as Marvell in providing an upper bound on label leakage from gradients. However, GAFM and Marvell are not mutually exclusive, and GAFM can incorporate optimized random noise provided by Marvell to enhance privacy protection. We provide an example on the Criteo dataset in Appendix F to demonstrate that combining GAFM and Marvell offers a better mitigation of LLG compared to using GAFM or Marvell alone, albeit with a slight decrease in utility. Another consideration is whether the distinct features observed in binary classification tasks, such as notable differences between positive and negative instance gradients, persist in multi-class settings, and how to extend current methods to multi-class scenarios. This presents an exciting direction for future work.

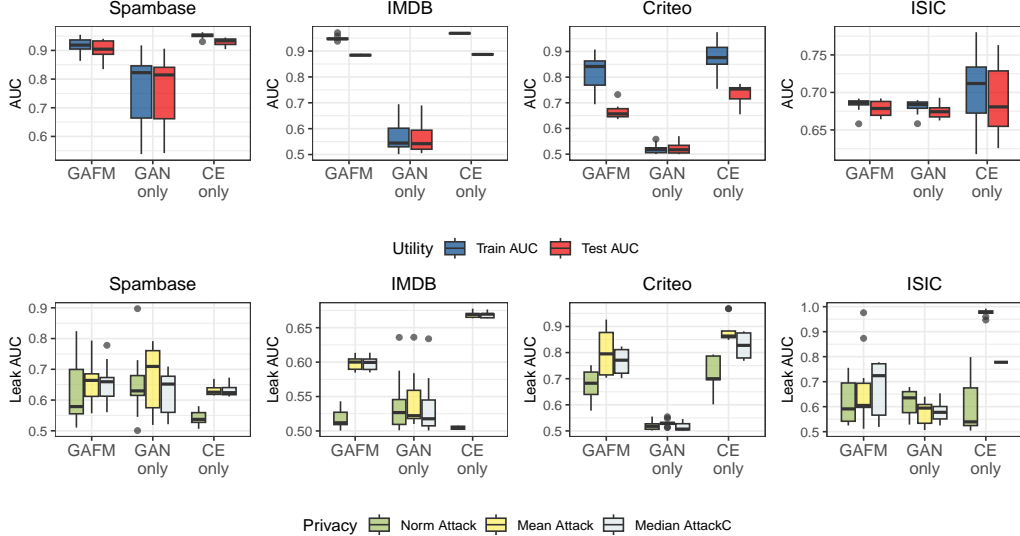


Figure 3: **Comparison of GAFM with two ablated versions:** GAN-only (GAFM with only GAN loss) and CE-only (GAFM with only CE loss). Figure 3 reveals that GAFM offers better trade-off between utility and privacy compared to the GAN-only model and the CE-only model. The GAN-only model achieves low leak AUC but has inferior classification AUC compared to GAFM. In contrast, the CE-only model fails to provide label privacy protection on most datasets. Figure 3 demonstrates the necessity of combining both the GAN and CE components.

References

- [1] Martin Abadi, Andy Chu, Ian Goodfellow, H Brendan McMahan, Ilya Mironov, Kunal Talwar, and Li Zhang. Deep learning with differential privacy. In *Proceedings of the 2016 ACM SIGSAC conference on computer and communications security*, pages 308–318, 2016.
- [2] Sharif Abuadbba, Kyuyeon Kim, Minki Kim, Chandra Thapa, Seyit A Camtepe, Yansong Gao, Hyoungshick Kim, and Surya Nepal. Can we use split learning on 1d cnn models for privacy preserving training? In *Proceedings of the 15th ACM Asia Conference on Computer and Communications Security*, pages 305–318, 2020.
- [3] Martin Arjovsky, Soumith Chintala, and Léon Bottou. Wasserstein generative adversarial networks. In *International conference on machine learning*, pages 214–223. PMLR, 2017.
- [4] Martin Arjovsky, Soumith Chintala, and Léon Bottou. Wasserstein generative adversarial networks. In Doina Precup and Yee Whye Teh, editors, *Proceedings of the 34th International Conference on Machine Learning*, volume 70 of *Proceedings of Machine Learning Research*, pages 214–223. PMLR, 06–11 Aug 2017.
- [5] David Byrd and Antigoni Polychroniadou. Differentially private secure multi-party computation for federated learning in financial applications. In *Proceedings of the First ACM International Conference on AI in Finance*, pages 1–9, 2020.
- [6] Iker Ceballos, Vivek Sharma, Eduardo Mugica, Abhishek Singh, Alberto Roman, Praneeth Vepakomma, and Ramesh Raskar. Splitnn-driven vertical partitioning. *arXiv preprint arXiv:2008.04137*, 2020.
- [7] Heng-Tze Cheng, Levent Koc, Jeremiah Harmsen, Tal Shaked, Tushar Chandra, Hrishi Aradhye, Glen Anderson, Greg Corrado, Wei Chai, Mustafa Ispir, Rohan Anil, Zakaria Haque, Lichan Hong, Vihan Jain, Xiaobing Liu, and Hemal Shah. Wide & deep learning for recommender systems, 2016.
- [8] Kewei Cheng, Tao Fan, Yilun Jin, Yang Liu, Tianjian Chen, Dimitrios Papadopoulos, and Qiang Yang. Secureboost: A lossless federated learning framework. *IEEE Intelligent Systems*, 36(6):87–98, 2021.
- [9] Matthew G Crowson, Dana Moukheiber, Aldo Robles Arévalo, Barbara D Lam, Sreekar Mantena, Aakanksha Rana, Deborah Goss, David W Bates, and Leo Anthony Celi. A systematic review of federated learning applications for biomedical data. *PLOS Digital Health*, 1(5):e0000033, 2022.
- [10] Ege Erdogan, Alptekin Kupcu, and A Ercument Cicek. Splitguard: Detecting and mitigating training-hijacking attacks in split learning. *arXiv preprint arXiv:2108.09052*, 2021.

- [11] Charlie Frogner, Chiyuan Zhang, Hossein Mobahi, Mauricio Araya, and Tomaso A Poggio. Learning with a wasserstein loss. *Advances in neural information processing systems*, 28, 2015.
- [12] Robin C Geyer, Tassilo Klein, and Moin Nabi. Differentially private federated learning: A client level perspective. *arXiv preprint arXiv:1712.07557*, 2017.
- [13] Ishaan Gulrajani, Faruk Ahmed, Martin Arjovsky, Vincent Dumoulin, and Aaron C Courville. Improved training of wasserstein gans. *Advances in neural information processing systems*, 30, 2017.
- [14] Otkrist Gupta and Ramesh Raskar. Distributed learning of deep neural network over multiple agents. *Journal of Network and Computer Applications*, 116:1–8, 2018.
- [15] Yoo Jeong Ha, Minjae Yoo, Gusang Lee, Soyi Jung, Sae Won Choi, Joongheon Kim, and Seehwan Yoo. Spatio-temporal split learning for privacy-preserving medical platforms: Case studies with covid-19 ct, x-ray, and cholesterol data. *IEEE Access*, 9:121046–121059, 2021.
- [16] Corentin Hardy, Erwan Le Merrer, and Bruno Sericola. Md-gan: Multi-discriminator generative adversarial networks for distributed datasets. In *2019 IEEE international parallel and distributed processing symposium (IPDPS)*, pages 866–877. IEEE, 2019.
- [17] Stephen Hardy, Wilko Henecka, Hamish Ivey-Law, Richard Nock, Giorgio Patrini, Guillaume Smith, and Brian Thorne. Private federated learning on vertically partitioned data via entity resolution and additively homomorphic encryption. *arXiv preprint arXiv:1711.10677*, 2017.
- [18] Briland Hitaj, Giuseppe Ateniese, and Fernando Perez-Cruz. Deep models under the gan: information leakage from collaborative deep learning. In *Proceedings of the 2017 ACM SIGSAC conference on computer and communications security*, pages 603–618, 2017.
- [19] Rui Hu, Yuanxiong Guo, Hongning Li, Qingqi Pei, and Yanmin Gong. Personalized federated learning with differential privacy. *IEEE Internet of Things Journal*, 7(10):9530–9539, 2020.
- [20] Leonid V Kantorovich. Mathematical methods of organizing and planning production. *Management science*, 6(4):366–422, 1960.
- [21] Oscar Li, Jiankai Sun, Xin Yang, Weihao Gao, Hongyi Zhang, Junyuan Xie, Virginia Smith, and Chong Wang. Label leakage and protection in two-party split learning. *arXiv preprint arXiv:2102.08504*, 2021.
- [22] Payman Mohassel and Yupeng Zhang. Secureml: A system for scalable privacy-preserving machine learning. In *2017 IEEE symposium on security and privacy (SP)*, pages 19–38. IEEE, 2017.
- [23] Vaikkunth Mugunthan, Vignesh Gokul, Lalana Kagal, and Shlomo Dubnov. Bias-free fedgan: A federated approach to generate bias-free datasets. *arXiv preprint arXiv:2103.09876*, 2021.
- [24] Stuart L Pardau. The california consumer privacy act: Towards a european-style privacy regime in the united states. *J. Tech. L. & Pol'y*, 23:68, 2018.
- [25] George-Liviu Pereteanu, Amir Alansary, and Jonathan Passerat-Palmbach. Split he: Fast secure inference combining split learning and homomorphic encryption. *arXiv preprint arXiv:2202.13351*, 2022.
- [26] Maarten G Poirot, Praneeth Vepakomma, Ken Chang, Jayashree Kalpathy-Cramer, Rajiv Gupta, and Ramesh Raskar. Split learning for collaborative deep learning in healthcare. *arXiv preprint arXiv:1912.12115*, 2019.
- [27] Mohammad Rasouli, Tao Sun, and Ram Rajagopal. Fedgan: Federated generative adversarial networks for distributed data. *arXiv preprint arXiv:2006.07228*, 2020.
- [28] Jiankai Sun, Xin Yang, Yuanshun Yao, and Chong Wang. Label leakage and protection from forward embedding in vertical federated learning. *arXiv preprint arXiv:2203.01451*, 2022.
- [29] Tom Titcombe, Adam J Hall, Pavlos Papadopoulos, and Daniele Romanini. Practical defences against model inversion attacks for split neural networks. *arXiv preprint arXiv:2104.05743*, 2021.
- [30] Praneeth Vepakomma, Otkrist Gupta, Tristan Swedish, and Ramesh Raskar. Split learning for health: Distributed deep learning without sharing raw patient data. *arXiv preprint arXiv:1812.00564*, 2018.
- [31] Paul Voigt and Axel Von dem Bussche. The eu general data protection regulation (gdpr). *A Practical Guide, 1st Ed., Cham: Springer International Publishing*, 10(3152676):10–5555, 2017.
- [32] Aidmar Wainakh, Fabrizio Ventola, Till Müßig, Jens Keim, Carlos Garcia Cordero, Ephraim Zimmer, Tim Grube, Kristian Kersting, and Max Mühlhäuser. User label leakage from gradients in federated learning. *arXiv preprint arXiv:2105.09369*, 2021.
- [33] Aidmar Wainakh, Fabrizio Ventola, Till Müßig, Jens Keim, Carlos Garcia Cordero, Ephraim Zimmer, Tim Grube, Kristian Kersting, and Max Mühlhäuser. User-level label leakage from gradients in federated learning. *Proceedings on Privacy Enhancing Technologies*, 2022(2):227–244, 2022.

- [34] Zhibo Wang, Mengkai Song, Zhifei Zhang, Yang Song, Qian Wang, and Hairong Qi. Beyond inferring class representatives: User-level privacy leakage from federated learning. In *IEEE INFOCOM 2019-IEEE Conference on Computer Communications*, pages 2512–2520. IEEE, 2019.
- [35] Yuezhou Wu, Yan Kang, Jiahuan Luo, Yuanqin He, and Qiang Yang. Fedcg: Leverage conditional gan for protecting privacy and maintaining competitive performance in federated learning. *arXiv preprint arXiv:2111.08211*, 2021.
- [36] Qiang Yang, Yang Liu, Yong Cheng, Yan Kang, Tianjian Chen, and Han Yu. Federated learning. *Synthesis Lectures on Artificial Intelligence and Machine Learning*, 13(3):1–207, 2019.
- [37] Xin Yang, Jiankai Sun, Yuanshun Yao, Junyuan Xie, and Chong Wang. Differentially private label protection in split learning. *arXiv preprint arXiv:2203.02073*, 2022.
- [38] Chengliang Zhang, Suyi Li, Junzhe Xia, Wei Wang, Feng Yan, and Yang Liu. {BatchCrypt}: Efficient homomorphic encryption for {Cross-Silo} federated learning. In *2020 USENIX Annual Technical Conference (USENIX ATC 20)*, pages 493–506, 2020.
- [39] Zhaohua Zheng, Yize Zhou, Yilong Sun, Zhang Wang, Boyi Liu, and Keqiu Li. Applications of federated learning in smart cities: recent advances, taxonomy, and open challenges. *Connection Science*, 34(1):1–28, 2022.
- [40] Ligeng Zhu, Zhijian Liu, and Song Han. Deep leakage from gradients. *Advances in Neural Information Processing Systems*, 32, 2019.

A GAFM Algorithm Description

The details of GAFM are outlined in Algorithm A.1.

Algorithm A.1 Generative Adversarial Federated Model

Input: Training data X_1, X_2, \dots, X_P , training labels Y , sample $u \sim \text{Uniform}(0, \Delta)$, $\varepsilon \sim \mathcal{N}(0, \sigma^2)$, epoch T , weight γ , learning rates $\alpha_d, \alpha_g, \alpha_L$, and clip value c .

Output: Updated intermediate results $f(X)$.

```

1: Initialize model parameters  $\theta_d^0, \theta_g^0$ , and  $\theta_p^0$  and calculate the initialized intermediate result  $f(X)$ .
2: while Not converged do
3:   Label party
4:   Step 1: Update the discriminator
5:   The label party computes the prediction  $\hat{Y} \leftarrow G_{\theta_g}(f(X))$  and updates the discriminator by  $\theta_d \leftarrow \theta_d + \alpha_d \nabla_{\theta_d} L_{\text{GAN}}$  and clip  $\theta_d \leftarrow \text{clip}(\theta_d, -c, c)$ .
6:   Step 2: Update the generator
7:   Then the label party updates the generator by  $\theta_g \leftarrow \theta_g - \alpha_g \nabla_{\theta_g} L_{\text{GAN}}$ .
8:   Step 3: Back-propagation
9:   The label party backpropagates normalized gradients with respect to  $f(X)$  to the passive parties:  $\text{grad}_{f(X)} = \gamma \frac{\nabla_{f(X)} L_{\text{GAN}}}{\|\nabla_{f(X)} L_{\text{GAN}}\|_2} + \frac{\nabla_{f(X)} L_{\text{CE}}}{\|\nabla_{f(X)} L_{\text{CE}}\|_2}$ .
10:  Non-label parties
11:  for  $p = 1$  to  $P$  do
12:    Step 4: Update local models
13:    Based on the locally model and  $\text{grad}_{f(X)}$ , passive party  $p$  updates  $\theta_p$ .
14:  end for
15: end while
16: Step 5: Forward-propagation
17: Update intermediate results  $f(X) \leftarrow \sum_{p=1}^P f_{\theta_p}(X_p)$ .

```

B Heuristic Justification for Improved Gradients Mixing

In this section, we provide a heuristic justification for why the GAN and CE components in GAFM tend to have opposite directions.

- To simplify the notation, we assume that the intermediate result $f(X) \in \mathbb{R}^d$, where $d = 1$ (the same heuristic justification can be easily applied for $d \neq 1$), and we follow the experimental setting by using the identity function $I(\cdot)$ as the transformation function $F(\cdot)$.
- We assume that $\sigma(f(X))$ (also $f(X)$) to be increase with Y since it tries to match \hat{Y} , which tends to increase with Y itself.

To optimize the equation (6), for the sample i , the intermediate gradient is:

$$\frac{\partial L_{\text{GAFM}}}{\partial f(X_i)} = \gamma \frac{\partial L_{\text{GAN}}}{\partial f(X_i)} + \frac{\partial L_{\text{CE}}}{\partial f(X_i)}. \quad (\text{B.1})$$

For the first term of equation (B.1) and assume the sample size N :

$$\frac{\partial L_{\text{GAN}}}{\partial f(X_i)} = -\frac{\partial D_{\theta_d}(G_{\theta_g}(f(X_i)))}{N \partial f(X_i)} = -\frac{\partial D_{\theta_d}(\hat{Y}_i)}{N \partial \hat{Y}_i} \frac{\partial \hat{Y}_i}{\partial f(X_i)}. \quad (\text{B.2})$$

- Consider the original GAN loss L_{GAN} and approximate it roughly with Taylor expansion and $\hat{Y} \rightarrow Y + \varepsilon$:

$$\begin{aligned}
L_{\text{GAN}}(\theta_d, \theta_g; \varepsilon) &= \mathbb{E}[D_{\theta_d}(Y + \varepsilon)] - \mathbb{E}[D_{\theta_d}(G_{\theta_g}(f(X_i)))] \\
&= \mathbb{E}_{Y=1}[D_{\theta_d}(1 + \varepsilon) - D_{\theta_d}(\hat{Y})] + \mathbb{E}_{Y=0}[D_{\theta_d}(\varepsilon) - D_{\theta_d}(\hat{Y})] \\
&\approx \mathbb{E}_{Y=1}[\nabla D_{\theta_d}(\hat{Y})(1 + \varepsilon - \hat{Y})] + \mathbb{E}_{Y=0}[\nabla D_{\theta_d}(\hat{Y})(\varepsilon - \hat{Y})] \\
&\approx \mathbb{E}_{Y=1}[\nabla D_{\theta_d}(\hat{Y})(1 - \hat{Y})] - \mathbb{E}_{Y=0}[\nabla D_{\theta_d}(\hat{Y})\hat{Y}].
\end{aligned} \quad (\text{B.3})$$

Hence, heuristically, $\nabla D_{\theta^d}(\hat{Y}_i)$ tends to be positive and large if \hat{Y}_i is large, whereas $\nabla D_{\theta^d}(\hat{Y}_i)$ tends to be small and negative if \hat{Y}_i is small. Since \hat{Y} is increasing with Y , we tend to have (1) $\frac{\partial \hat{Y}}{\partial f(X)} > 0$, and (2) and $\nabla D_{\theta^d}(\hat{Y}_1) - \nabla D_{\theta^d}(\hat{Y}_0) > 0$, where \hat{Y}_1, \hat{Y}_0 represent some \hat{Y} from class 1 and class 0 respectively. Hence, $\frac{\partial L_{\text{GAN}}}{\partial f_1(X)}$ tend to be smaller than $\frac{\partial L_{\text{GAN}}}{\partial f_0(X)}$ where $f_1(X), f_0(X)$ represent some $f(X)$ from class 1 and class 0. This is GAN loss gradients of GAFM we observed in figure 2, figure C.1 and figure C.2.

- Consider the original GAN loss L_{GAN} and approximate it roughly with Taylor expansion and $\hat{Y} \rightarrow 1 - (Y + \varepsilon)$, we have the similar conclusion as equation B.3. Since \hat{Y} is decreasing with Y , we tend to have (1) $\frac{\partial \hat{Y}}{\partial f(X)} < 0$, and (2) and $\nabla D_{\theta^d}(\hat{Y}_0) - \nabla D_{\theta^d}(\hat{Y}_1) > 0$. Hence, we still have $\frac{\partial L_{\text{GAN}}}{\partial f_1(X)}$ tend to be smaller than $\frac{\partial L_{\text{GAN}}}{\partial f_0(X)}$.

For the second term of equation (B.1): let $S_i = \sigma(f(X_i))$ and $\frac{\partial S_i}{\partial f(X_i)} > 0$, hence,

$$\frac{\partial L_{\text{CE}}}{\partial f(X_i)} = \frac{1}{N} \left(-\frac{\tilde{Y}}{S_i} + \frac{1 - \tilde{Y}}{1 - S_i} \right) \frac{\partial S_i}{\partial f(X_i)} \propto \frac{1}{N} \frac{S_i - \tilde{Y}}{S_i(1 - S_i)}. \quad (\text{B.4})$$

Without the GAN loss part, in a perfectly fitted model, we tend to have,

$$\begin{cases} \mathbb{E}(S_i|Y_i = 1) = \mathbb{E}(\tilde{Y}_i|Y_i = 1) = 0.5 + \frac{\Delta}{2} \\ \mathbb{E}(S_i|Y_i = 0) = \mathbb{E}(\tilde{Y}_i|Y_i = 0) = 0.5 - \frac{\Delta}{2} \end{cases}. \quad (\text{B.5})$$

In practice, an imperfect fit tends to have $E(\tilde{Y}_i|Y_i = 1) < E(\dot{Y}_i|Y_i = 1)$ and $E(\tilde{Y}_i|Y_i = 0) > E(\dot{Y}_i|Y_i = 0)$. In addition, with the GAN loss part, the larger gradient (usually) for $Y = 0$ from the GAN loss drives \tilde{Y}_i to decrease more at $Y = 0$ compared to that from $Y = 1$. Combining them together, heuristically, we tend to have,

$$\frac{\partial L_{\text{CE}}}{\partial f(X_i)} \propto \begin{cases} \frac{1}{N} \frac{S_i - \tilde{Y}}{S_i(1 - S_i)} > 0; & Y_i = 1 \\ \frac{1}{N} \frac{S_i - \tilde{Y}}{S_i(1 - S_i)} < 0; & Y_i = 0 \end{cases} \quad (\text{B.6})$$

This is CE loss gradients of GAFM we observed in figure C.1 and figure 2.

Finally, combining equations (B.2) and (B.6), when $\hat{Y} \rightarrow Y + \varepsilon$, the normalized final gradient for L_{GAFM} is

$$\frac{\partial L_{\text{GAFM}}}{\partial f(X_i)} = \begin{cases} \gamma \frac{-\nabla D_{\theta^d}(\hat{Y}_i) \frac{\partial \hat{Y}_i}{\partial f(X_i)}}{\|\nabla D_{\theta^d}(\hat{Y}) \frac{\partial \hat{Y}}{\partial f(X)}\|_2} \downarrow + \frac{\frac{S_i - \tilde{Y}}{N S_i (1 - S_i)} \frac{\partial S_i}{\partial f(X_i)}}{\|\frac{S_i - \tilde{Y}}{N S_i (1 - S_i)} \frac{\partial S_i}{\partial f(X)}\|_2} \uparrow; & Y = 1 \\ \gamma \frac{-\nabla D_{\theta^d}(\hat{Y}_i) \frac{\partial \hat{Y}_i}{\partial f(X_i)}}{\|\nabla D_{\theta^d}(\hat{Y}) \frac{\partial \hat{Y}}{\partial f(X)}\|_2} \uparrow + \frac{\frac{S_i - \tilde{Y}}{N S_i (1 - S_i)} \frac{\partial S_i}{\partial f(X_i)}}{\|\frac{S_i - \tilde{Y}}{N S_i (1 - S_i)} \frac{\partial S_i}{\partial f(X)}\|_2} \downarrow; & Y = 0 \end{cases}, \quad (\text{B.7})$$

where the normalization operation preserves the order of gradients. By equation B.7, our heuristic analysis suggests that the gradients from the GAN component and the CE component tend to have opposite directions, resulting in the mutual perturbation of the gradients of both the GAN loss and the CE loss, leading to a better blending of the overall gradient.

C Complete Experimental Results

C.1 Intermediate Gradients on Additional Datasets

Figures C.1, C.2, and C.3 show the intermediate gradients of Spambase, Criteo, and ISIC datasets, respectively. Consistent with the results on the IMDB dataset, we observe that GAFM has more mixed gradients compared to Vanilla on these three datasets. These observation support the analysis in Appendix B that the mixed gradients of GAFM can be attributed to the mutual cancellation between GAN loss gradients and CE loss gradients.

C.2 Evaluation in the Multi-Party Setting

In this section, we extend the two-party split learning setting to the multi-party split learning setting, where three non-label parties and one label party collaborate to train GAFM. We evaluate two scenarios for local feature assignment: balanced and imbalanced. For Spambase and Criteo datasets, the local feature assignment ratio among the three participants is set to $client_1 : client_2 : client_3 = 1 : 1 : 1$, while for IMDB dataset, it is set to $client_1 : client_2 : client_3 = 2 : 2 : 1$. Since ISIC image dataset is not suitable for multi-party scenarios, we exclude it from our

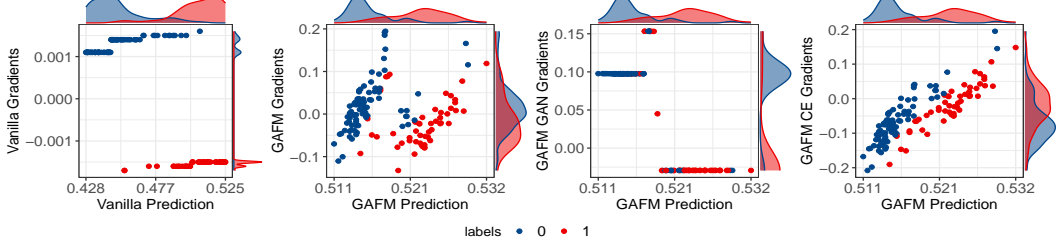


Figure C.1: Comparison of Prediction vs. Intermediate Gradients between vanilla SplitNN and GAFM on Spambase. The figure displays, from left to right, the intermediate gradients of vanilla SplitNN, GAFM, the GAN loss gradient of GAFM, and the CE loss gradient of GAFM. We observe that the mutual perturbation between the GAN loss gradient and the CE loss gradient generate intermediate gradients that are more mixed compared to vanilla SplitNN.

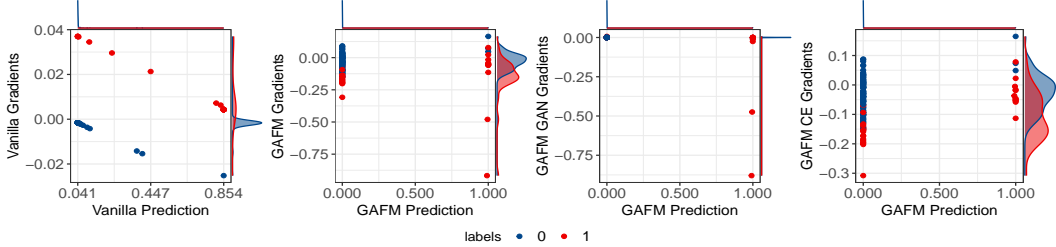


Figure C.2: Comparison of Prediction vs. Intermediate Gradients between vanilla SplitNN and GAFM on Criteo. The figure displays, from left to right, the intermediate gradients of vanilla SplitNN, GAFM, the GAN loss gradient of GAFM, and the CE loss gradient of GAFM. We observe that the mutual perturbation between the GAN loss gradient and the CE loss gradient generate intermediate gradients that are more mixed compared to vanilla SplitNN.

experiments. The experimental setup is consistent with that of section 4.1, with the exception of the transformation function $F(\cdot)$. In this case, $F(\cdot)$ is an averaging function rather than the identity function $I(\cdot)$.

$$f(X) = F(f(X_1), f(X_2), f(X_3)) = \frac{f(X_1) + f(X_2) + f(X_3)}{3}. \quad (\text{C.1})$$

where $f(X_i)$ is the intermediate results from the i th non-label party.

The leak AUC in Tabel C.1 measures not only the overall leakage, but also the leakage of each non-label party, as the \tilde{y}_1 , \tilde{y}_2 , and \tilde{y}_3 are equally weighted at the cut layer. We observe that the utility of both GAFM and Marvell slightly decreases in the multi-party setting compared to the two-party setting, possibly due to the increased difficulty of jointly training with multiple participants. However, in the multi-client setting, GAFM still achieves a better trade-off between utility and privacy compared to all baselines.

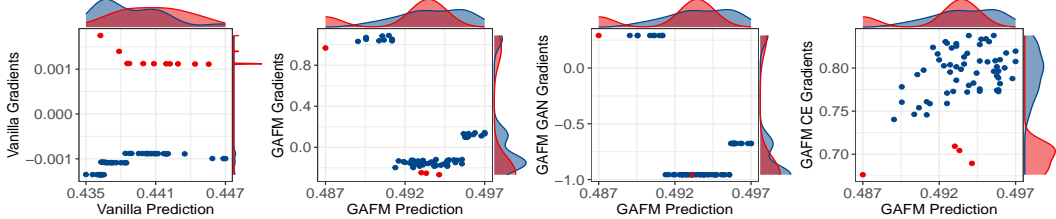


Figure C.3: Comparison of Prediction vs. Intermediate Gradients between vanilla SplitNN and GAFM on ISIC. The figure displays, from left to right, the intermediate gradients of vanilla SplitNN, GAFM, the GAN loss gradient of GAFM, and the CE loss gradient of GAFM. We observe that the mutual perturbation between the GAN loss gradient and the CE loss gradient generate intermediate gradients that are more mixed compared to vanilla SplitNN.

Table C.1: Comparison of utility and privacy on multi-party setting over 10 repetitions. In the multi-party setting, GAFM still outperforms Vanilla and Max Norm in terms of privacy preservation, and Marvell in terms of utility.

| dataset | Method | Training AUC | Testing AUC | Norm Attack | Mean Attack | Median Attack |
|----------|----------|--------------|-------------|-------------|-------------|---------------|
| Spambase | GAFM | 0.87±0.15 | 0.86±0.15 | 0.60±0.07 | 0.69±0.06 | 0.68±0.07 |
| | Marvell | 0.70±0.05 | 0.68±0.06 | 0.53±0.03 | 0.70±0.02 | 0.70±0.02 |
| | Max Norm | 0.95±0.00 | 0.95±0.00 | 0.83±0.11 | 0.99±0.02 | 0.99±0.04 |
| | Vanilla | 0.95±0.00 | 0.95±0.00 | 0.84±0.13 | 1.00±0.00 | 1.00±0.00 |
| IMDB | GAFM | 0.97±0.01 | 0.82±0.00 | 0.54±0.02 | 0.65±0.04 | 0.54±0.02 |
| | Marvell | 0.82±0.01 | 0.78±0.01 | 0.51±0.01 | 0.71±0.02 | 0.71±0.02 |
| | Max Norm | 0.97±0.00 | 0.88±0.00 | 0.54±0.03 | 0.99±0.01 | 1.00±0.00 |
| | Vanilla | 0.97±0.00 | 0.88±0.00 | 0.54±0.02 | 0.99±0.01 | 1.00±0.00 |
| Criteo | GAFM | 0.80±0.01 | 0.65±0.02 | 0.63±0.01 | 0.86±0.01 | 0.80±0.00 |
| | Marvell | 0.83±0.03 | 0.70±0.04 | 0.75±0.08 | 0.85±0.09 | 0.78±0.04 |
| | Max Norm | 0.83±0.02 | 0.71±0.02 | 0.91±0.03 | 0.95±0.09 | 0.82±0.00 |
| | Vanilla | 0.83±0.02 | 0.71±0.02 | 0.91±0.03 | 0.95±0.09 | 0.82±0.00 |

Table D.1: Hyperparameters of GAFM on four datasets. The following section discusses the selection of three crucial parameters in GAFM: σ (section D.1), γ (section D.2), and Δ (section D.3), respectively.

| Dataset | σ | Δ | γ |
|----------|----------|----------|----------|
| Spambase | 0.01 | 0.05 | 1 |
| IMDB | 0.01 | 0.1 | 1 |
| Criteo | 0.01 | 0.5 | 1 |
| ISIC | 0.01 | 0.05 | 20 |

D Discussion on hyperparameters

In this section, we present the methods for selecting the key hyperparameters σ , γ , and Δ in GAFM. Table D.1 presents the hyperparameters of GAFM that are utilized in our experiments on four datasets.

D.1 Discussion on σ

We conducted a comparison of GAFM with varying values of σ over 10 repetitions, as shown in Table D.2. Our results indicate that a moderately large σ does not significantly compromise prediction accuracy and can still offer robust protection against label stealing attacks. Thus, we have chosen to fix σ at 0.01 for all datasets.

D.2 Discussion on γ

We use the loss weight parameter γ to balance the GAN and CE loss gradients in GAFM, allowing them to effectively perturb each other. Table D.3 shows the average gradients of the GAN and CE losses for the GAFM model on four datasets, with $\gamma = 1$ and other hyperparameters consistent with the section 4.1. The results indicate that the mean gradients of the GAN and CE losses are similar in magnitude for the Spambase, IMDB, and Criteo datasets, but the CE loss gradient is over 10 times larger than the GAN loss gradient for the ISIC dataset. This explains why Spambase, IMDB, and Criteo can achieve satisfactory utility-privacy trade-offs with $\gamma = 1$, while ISIC requires a higher value of γ .

We further discuss how to select the appropriate value of γ for the ISIC dataset. Based on the results shown in Table D.3, the value of γ should ideally be in the range of 10 to 20. We set the parameter Δ to a minimum value of 0.05 to control its impact on privacy and utility while keeping all other parameters and experimental settings unchanged. Table D.4 reports the experimental results of GAFM’s privacy and utility under different values of γ . GAFM achieves comparable average training AUC and test AUC on the ISIC 10% subset across the range of γ values. However, at $\gamma = 20$, GAFM achieves the minimum average leak AUC under three different attacks. Therefore, we conclude that the optimal parameter for the ISIC subset is $\gamma = 20$.

To validate the effectiveness of the selected γ on the subset, we also report the experimental results on the full ISIC dataset with different values of γ in Table D.5. We find that $\gamma = 20$ is also an appropriate value for the full dataset. The

Table D.2: Average AUC and Leak AUC of GAFM with different σ . We observe that GAFM is insensitive to σ in terms of both utility and privacy.

| dataset | σ | Training AUC | Test AUC | Norm Attack | Mean Attack | Median Attack |
|----------|----------|--------------|-----------|-------------|-------------|---------------|
| Spambase | 0.01 | 0.94±0.01 | 0.93±0.02 | 0.56±0.04 | 0.67±0.05 | 0.66±0.05 |
| | 0.25 | 0.94±0.01 | 0.93±0.01 | 0.60±0.06 | 0.67±0.03 | 0.67±0.03 |
| | 1 | 0.94±0.01 | 0.94±0.01 | 0.57±0.05 | 0.68±0.04 | 0.68±0.04 |
| IMDB | 0.01 | 0.95±0.01 | 0.88±0.00 | 0.52±0.01 | 0.60±0.01 | 0.60±0.01 |
| | 0.25 | 0.92±0.14 | 0.85±0.11 | 0.52±0.02 | 0.60±0.03 | 0.61±0.03 |
| | 1 | 0.87±0.18 | 0.81±0.15 | 0.54±0.03 | 0.60±0.06 | 0.61±0.05 |
| Criteo | 0.01 | 0.82±0.07 | 0.67±0.03 | 0.68±0.06 | 0.80±0.09 | 0.77±0.05 |
| | 0.25 | 0.80±0.00 | 0.69±0.03 | 0.74±0.07 | 0.82±0.03 | 0.82±0.00 |
| | 1 | 0.81±0.02 | 0.66±0.03 | 0.71±0.08 | 0.82±0.02 | 0.82±0.00 |
| ISIC | 0.01 | 0.68±0.01 | 0.68±0.01 | 0.62±0.09 | 0.66±0.15 | 0.68±0.11 |
| | 0.25 | 0.68±0.01 | 0.67±0.01 | 0.63±0.06 | 0.69±0.13 | 0.69±0.09 |
| | 1 | 0.68±0.01 | 0.67±0.01 | 0.63±0.06 | 0.69±0.13 | 0.69±0.09 |

Table D.3: Results of the average GAN loss gradient and average CE loss gradient on the four datasets. It is observed that only for the ISIC dataset, the CE loss gradient mean and GAN loss gradient mean are not on the same scale. To better achieve gradient perturbation, an increase in γ for ISIC is necessary.

| dataset | (Δ, γ, σ) | GAN Gradient Avg. | CE Gradient Avg. | Comparable Magnitude |
|----------|----------------------------|-------------------|------------------|----------------------|
| Spambase | (0.05,1,0.01) | 0.054 | -0.049 | ✓ |
| IMDB | (0.05,1,0.01) | 0.006 | -0.006 | ✓ |
| Criteo | (0.05,1,0.01) | -0.011 | 0.048 | ✓ |
| ISIC | (0.05,1,0.01) | 0.058 | 0.789 | ✗ |

Table D.4: The impact of different γ values on the utility and privacy of GAFM on **the 10% subset ISIC data**. Table D.4 reports the experimental results of GAFM with various γ values, while maintaining all other experimental settings consistent. Moreover, we set the parameter Δ to a minimum value of 0.05 to control its effect on utility and privacy. Based on the overall assessment of utility and privacy, we conclude that the optimal value for γ is 20.

| γ | (Δ, σ) | Training AUC | Test AUC | Norm Attack | Mean Attack | Median Attack |
|----------|--------------------|--------------|-----------|-------------|-------------|---------------|
| 1 | (0.05,0.01) | 0.65±0.06 | 0.65±0.06 | 0.77±0.04 | 0.99±0.01 | 0.78±0.00 |
| 10 | (0.05,0.01) | 0.67±0.03 | 0.66±0.05 | 0.77±0.04 | 0.98±0.02 | 0.78±0.00 |
| 15 | (0.05,0.01) | 0.67±0.03 | 0.66±0.05 | 0.76±0.04 | 0.96±0.04 | 0.77±0.00 |
| 20 | (0.05,0.01) | 0.67±0.03 | 0.66±0.05 | 0.76±0.04 | 0.93±0.05 | 0.76±0.00 |

Table D.5: The impact of different γ values on the utility and privacy of GAFM on **the full ISIC data**. Table D.4 reports the experimental results of GAFM with various γ values, while maintaining all other experimental settings consistent. Moreover, we set the parameter Δ to a minimum value of 0.05 to control its effect on utility and privacy. Based on the overall assessment of utility and privacy, we conclude that the optimal value for γ is 20.

| γ | (Δ, σ) | Training AUC | Test AUC | Norm Attack | Mean Attack | Median Attack |
|----------|--------------------|-----------------|-----------------|-----------------|-----------------|-----------------|
| 1 | (0.05, 0.01) | 0.67 \pm 0.02 | 0.66 \pm 0.03 | 0.98 \pm 0.01 | 0.97 \pm 0.02 | 0.78 \pm 0.00 |
| 10 | (0.05, 0.01) | 0.67 \pm 0.02 | 0.68 \pm 0.01 | 0.77 \pm 0.19 | 0.80 \pm 0.12 | 0.74 \pm 0.04 |
| 15 | (0.05, 0.01) | 0.67 \pm 0.04 | 0.66 \pm 0.05 | 0.61 \pm 0.07 | 0.66 \pm 0.15 | 0.68 \pm 0.09 |
| 20 | (0.05, 0.01) | 0.68 \pm 0.01 | 0.68 \pm 0.01 | 0.62 \pm 0.09 | 0.66 \pm 0.15 | 0.68 \pm 0.11 |

Table D.6: Average ratio results on the full dataset and small subset. For the ISIC dataset, the optimal Δ selected is consistent between the full dataset and 10% subset. Although for the Spambase, IMDB, and Criteo datasets, the optimal Δ selected differs between the full dataset and small subset, the selected ratio values are very close.

| dataset | sampling ratio | $\Delta = 0.05$ | $\Delta = 0.1$ | $\Delta = 0.2$ | $\Delta = 0.3$ | $\Delta = 0.5$ |
|----------|----------------|-----------------|----------------|----------------|----------------|----------------|
| Spambase | 1 | 0.727 | 0.733 | 0.722 | 0.723 | 0.746 |
| | 0.1 | 0.849 | 0.856 | 0.968 | 0.992 | 1.043 |
| IMDB | 1 | 0.627 | 0.648 | 0.895 | 0.833 | 0.833 |
| | 0.1 | 1.189 | 1.076 | 1.323 | 1.158 | 1.309 |
| Criteo | 1 | 1.061 | 0.941 | 1.226 | 0.993 | 1.011 |
| | 0.1 | 1.359 | 1.342 | 1.331 | 1.328 | 1.306 |
| ISIC | 1 | 0.933 | 0.955 | 0.990 | 1.009 | 1.022 |
| | 0.1 | 1.234 | 1.246 | 1.238 | 1.243 | 1.241 |

consistency of the selected γ for both the subset and the full dataset demonstrates the validity of determining γ based on sampling.

D.3 Discussion on Δ

We now turn to the topic of determining the randomized response-related hyperparameter Δ in GAFM. In section 4.1, we chose Δ based on the measure $Ratio = \frac{leakAUC}{trainAUC}$ and the minimum average ratio criterion. Specifically, we selected Δ that yields the lowest average ratio across all three attacks.

We follow the procedure outlined below. After fixing the other parameters, we only randomly sample a small subset (10%) of the dataset without replacement to ensure privacy, which is shared between the label and non-label parties. GAFM is trained on this small subset with different values of Δ , and we repeat this process 5 times. We then compute the ratio of norm attack, mean attack, and median attack for each value of Δ and average these ratios across the repetitions. The results are presented in Table D.6. Based on these ratios, we select the optimal Δ for each dataset subset. Specifically, the optimal Δ for the Spambase subset is 0.05, for the IMDB subset is 0.1, for the Criteo subset is 0.5, and for the ISIC subset is 0.05.

To better demonstrate the effectiveness of the ratio-based strategy, we compare the detailed ratios on both the full dataset and the small subset in Table D.6. Our observation shows that the optimal Δ selected based on the ratio results from the small subset is consistent with that selected based on the full dataset experiment results for the ISIC dataset. For Spambase, IMDB, and Criteo datasets, the optimal Δ selected based on the ratio results from the small subset is very close to that selected based on the full dataset in terms of the average ratio value. Figure D.1 further visualizes this degree of closeness, where the three colored blocks on the full dataset represent the three sets of parameters with the smallest ratio. We find that the optimal parameter (red block) selected on the small subset is always included in the three sets of parameters with the smallest ratio on the full dataset.

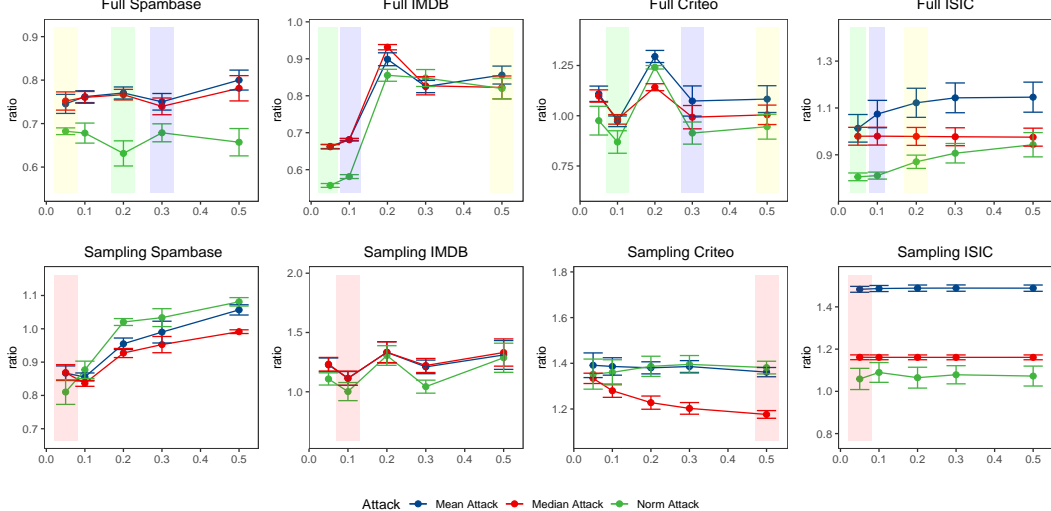


Figure D.1: The ratio distribution on the full dataset and small subset. In Figure D.1, the green (smallest), blue (second smallest), and orange (third smallest) blocks correspond to the three smallest ratio values on the full dataset for different Δ , while the red block represents Δ with the smallest average ratio on the small subset. Notably, we observe that Δ with the smallest average ratio on the small subset always belongs to the three groups of Δ with the smallest average ratio on the full dataset.

E Data setup and Experiment Details

In this section, we provide a detailed overview of our experimental setup. We first describe the pre-processing steps for the four public datasets in E.1. Next, we provide a description of the model architecture used for each dataset in E.2. Finally, we present the training hyperparameters for each dataset and model combination in E.3.

E.1 Dataset Processing

Spambase Spambase data are classified as whether they are spam or not. The Spambase dataset contains 4061 instances, each with 55 continuous real attributes and 2 continuous integer attributes. To preprocess the data, we replace all NA values with 0 and normalize the features to reduce the impact of magnitude differences. During each repetition, we split the dataset into a 70%-30% train-test split at different random seed settings.

IMDB The IMDB data has been preprocessed and words are encoded as a sequence of word indexes in the form of integers. We select the top 500 words and encode indexes with one-hot. The 50000 reviews are split into 25000 for training and 25000 for testing at different random seeds. And the final training and test data are both 25000×500 matrices filled with 0s and 1s.

Criteo The Criteo dataset consists of a portion of Criteo’s traffic over a period of 7 days. Each row corresponds to a display ad served by Criteo. The dataset comprises 13 integer features and 26 categorical features, all of which have been hashed onto 32 bits. We followed the winner of the Criteo Competition’s recommendations for data preprocessing⁵ and the code⁶ to process the entire dataset, rather than just a 10% subset like the Marvell paper. Our preprocessing steps included removing infrequent features that appeared in less than 10 instances, transforming numerical features (I1-I13) into categorical features, and treating them as a single feature. Additionally, we discretized numerical values using \log_2 transformation. For each iteration, we split the dataset into an 80%-20% train-test split using different random seed settings.

ISIC The official SIIM-ISIC Melanoma Classification dataset contains a total of 33126 skin lesion images, with less than 2% positive examples. To preprocess the ISIC data, we followed the approach outlined in this code⁷. During each iteration, we revise the image size $64 \times 64 \times 1$ and randomly split the dataset into an 80%-20% train-test split, using different random seed settings for each split.

⁵<https://www.csie.ntu.edu.tw/~r01922136/kaggle-2014-criteo.pdf>

⁶<https://github.com/rixwew/pytorch-fm/blob/master/torchfm/dataset/criteo.py>

⁷https://github.com/OscarcarLi/label-protection/blob/main/preprocess_ISIC.ipynb

E.2 Model Architecture Details

To maintain consistency across all datasets, we utilized a 2-layer DNN as the generator and discriminator for our GAFM model. The intermediate results $f(X)$ were already transformed into linear embeddings, making them easily handled by the 2-layer DNN. For the generator and discriminator, we used LeakyReLU as the activation function for all layers except for the generator’s output layer, which used the Sigmoid activation function. In the following sections, we will discuss the specific local model architectures used for feature extraction on each dataset.

Spambase For the Spambase dataset, the local model architecture consists of two linear layers with a LeakyReLU activation function. The first layer transforms the input size to a hidden representation of $batchsize \times 16$, and the second layer maps the hidden representation to a one-dimensional output using a sigmoid function.

IMDB The local model architecture for the IMDB dataset is a fully connected model with 3 linear layers. The model consists of two hidden layers with 256 and 128 units, respectively, followed by ReLU activation functions and a dropout rate of 0.5. The output layer has a single unit after a sigmoid function.

Criteo In the context of online advertising data from Criteo, we utilize a widely-used deep learning model architecture called Wide and Deep model [7]. To implement Wide and Deep model, we refer to the code⁸. The architecture of Wide and Deep model consists of three main components: FeaturesLinear, FeaturesEmbedding, and MultiLayerPerceptron. The FeaturesLinear module is a linear model that uses embedding layers and a bias term to model feature interactions. The embeddings have a desired output dimension of 1. And the FeaturesEmbedding and MultiLayerPerceptron components take embedding layers as input features and uses a series of fully connected layers to learn complex feature interactions. In this implementation, the embedding dimension is set to 16 and the MLP dimension is set to 16×16 . These components are combined in the local model, which adds a linear output layer with an output dimension of 1.

ISIC The local model for ISIC consists of 3 convolutional layers with 6, 16, and 32 output channels respectively. Each convolutional layer uses a 3×3 filter with a stride of 1×1 . Following each convolutional layer is a ReLU activation function, and the output of each activation is max-pooled with a 2×2 window and stride size of 2×2 . The output of the third convolutional layer is then flattened into size $32 \times 6 \times 6$ and passed into 3 fully connected layers, with 120, 84, and 40 units respectively.

E.3 Model Training Details

We set the transformation function $F(\cdot)$ to the identity function $I(\cdot)$, clip the value at $c = 0.1$, use random seeds from 0 to 9. We employ PyTorch with CPU for Spambase and IMDB and employ PyTorch with CUDA acceleration to conduct all experiments for Criteo and ISIC. The Spambase dataset takes approximately 10 minutes per repetition, while the IMDB dataset requires around 0.5 hours. For the Criteo dataset, each repetition takes about 2.5 hours, and for the ISIC dataset, it takes about 40 minutes per repetition.

Spambase, IMDB We use the Adam optimizer with a batch size of 1028 and a learning rate of 1e-4 throughout the entire training of 300 epochs.

Criteo We use the Adam optimizer with a batch size of 256 and a learning rate of 1e-4 throughout the entire training of 100 epochs.

ISIC We use the Adam optimizer with a batch size of 256 and a learning rate of 1e-6 throughout the entire training of 250 epochs.

F The Combination of GAFM and Marvell

In this section, we use the Criteo dataset as an example to demonstrate that combining GAFM and Marvell can enhance the privacy protection of GAFM. Table F.1 shows the utility and privacy of GAFM, Marvell, and their combination (referred to as the G-M model) on the Criteo dataset, with the same experiment setup as the section 4.1. We observe a significant decrease in the leak AUC of the G-M model compared to Marvell and GAFM, demonstrating its improved ability to mitigate LLG.

⁸https://github.com/BrandonCXY/Pytorch_RecommenderSystem/blob/master/DL%20Models%20Implementation%20in%20Recommender%20Sys%20with%20Pytorch.py

Table F.1: An example of the combination of GAFM and Marvell on Criteo. Table F.1 demonstrates that the G-M model outperforms GAFM and Marvell in terms of lower leak AUC, indicating a better ability to protect label privacy, despite some utility degradation.

| Method | Utility | | | Privacy | | |
|---------|-------------|--------------|-------------|----------------|----------------|------------------|
| | Avg. AUC | Worst AUC | Best AUC | Norm Attack | Mean Attack | Median Attack |
| GAFM | 0.67 | 0.64 | 0.73 | 0.68±0.06 | 0.80±0.09 | 0.77±0.05 |
| Marvell | 0.70 | 0.65 | 0.76 | 0.76±0.08 | 0.86±0.08 | 0.78±0.04 |
| G-M | 0.64 | 0.62 | 0.65 | 0.60±0.02 | 0.66±0.01 | 0.65±0.01 |